Available online at www.sciencedirect.com
SCIENCE DIRECT®
Journal of Colloid and Interface Science 273 (2004) 278–290
JOURNAL OF Colloid and Interface Science
www.elsevier.com/locate/jcis

Electrostatic double-layer interaction between spherical particles inside a rough capillary

Prodip K. Das and Subir Bhattacharjee *

Department of Mechanical Engineering, 4–9 Mechanical Engineering Building, University of Alberta, Edmonton, AB T6G 2G8, Canada

Received 1 July 2003; accepted 1 October 2003

Abstract

Predictions of electrostatic double-layer interaction forces between two similarly charged spherical colloidal particles inside an infinitely long "rough" capillary are presented. A simple model of a rough cylindrical surface is proposed, which assumes the capillary wall to be a periodic function of axial position. The periodic roughness of the wall is characterized by the wavelength and amplitude of the undulations. The electrostatic double-layer interaction force between two spherical particles located axially inside this rough capillary is determined by solving the nonlinear Poisson–Boltzmann equation employing finite element analysis. The effect of surface roughness of the cylindrical enclosure on the interaction force between two particles is extensively studied on the basis of this model. The simulations are carried out for dimensionless amplitudes (amplitude/particle radii) ranging from 0.05 to 0.15 and scaled wavelengths (wavelength/particle radii) ranging from 0.4 to 4.0. The interaction force between the particles is significantly modified by the proximity of the rough capillary wall. Generally, the interaction force for rough capillaries oscillates around the corresponding interaction force in a smooth capillary depending on the magnitudes of the scaled amplitude and wavelength of the roughness. The influence of roughness on the electrostatic interactions becomes more pronounced when the surface potential of the cylinder wall is different from the sphere surface potentials. When the cylinder and the particle surfaces have large potential differences, the axial force experienced by a particle is dominated by the capillary roughness. There are dramatic oscillations of the force, which alternately becomes repulsive and attractive as the particle moves from the crest to the trough of the rough capillary wall. These results suggest that manipulation of colloidal particles in narrow microchannels may be subject to significant force variations owing to the roughness inherent in microfabricated channels etched on metal films.

Keywords: Colloidal particle; Cylindrical capillary; Electrostatic interaction; Nonlinear Poisson–Boltzmann equation; Surface roughness; Finite element analysis

1. Introduction

The interaction force between colloidal particles, generally obtained in the Derjaguin–Landau–Verwey–Overbeek (DLVO) construct [1,2], is extensively used to describe natural and industrial processes involving colloidal particles, for instance, flow through porous media, microfluidic actuation, capillary electrophoresis, and chromatographic separations [3,4]. The DLVO model provides the pair interaction between two charged colloidal objects in an infinite electrolytic domain. Several applications, particularly those involving particles in a confined domain, such as porous media, likely violate the limitations imposed by such a pair-potential approach. In these cases, the pore walls will modify the net interaction force between the colloidal particles trapped inside the pore. Furthermore, in most natural processes, the confining pore geometry is extremely heterogeneous. Morphological heterogeneity, or roughness, is already considered a key factor in seriously altering the DLVO interaction energy and force between colloidal objects [4,5]. It is believed that the effect of surface roughness on both the Lifshitz–van der Waals (LW) and the electrostatic double-layer (EDL) forces, the two components of the DLVO interaction force [6], is substantial. For instance, surface roughness is typically considered as a possible cause for the large discrepancies observed between the theoretical predictions and experimental observations in particle deposition, heterocoagulation, colloidal fouling of surfaces, and various other engineered and natural processes [7–14].

During the past several decades, considerable attention has been devoted toward accurate prediction of colloidal

* Corresponding author.
E-mail address: subir.b@ualberta.ca (S. Bhattacharjee).

0021-9797/$ – see front matter
doi:10.1016/j.jcis.2003.10.003

interactions for various geometries, for instance, particle–particle interaction in an infinite domain, particle–plate interaction, and interaction between a particle and cylindrical capillary [15–20]. However, particle–particle interactions in confined domains have not been studied as rigorously. While it might be pertinent to assume pairwise additivity of dispersion forces and calculate the net LW interaction in such systems by a simple extension of Hamaker's microscopic approach [21], calculations of the net electrostatic double-layer interaction in such confined geometries is considerably more difficult. In a confined system, the presence of charge on the confining walls alters the electrolyte distribution inside the domain, which in turn influences the net interaction between two colloidal particles in the confinement. Furthermore, if the walls of the confinement are rough, the electrolyte distribution is perturbed locally, which can cause further complications. The overall consequence is that the EDL interactions between colloidal particles in complex confined geometries cannot possibly be determined by simple pairwise summation procedures.

The objective of the present work is to obtain the electrostatic double-layer interaction force between two spherical colloidal particles trapped inside a cylindrical capillary of comparable dimension, with a periodic undulation present on the capillary wall. This problem is a simple mathematical construct to assess the coupled influence of the charged capillary wall, and the surface roughness of the wall on the electrostatic interaction between the colloidal particles. The importance of considering roughness on confining walls of a capillary stems from our ongoing attempts to analyze the flow of particles inside microscopic microfluidic channels. In these microfluidic processes, we apply an electrical potential on the channel wall to induce movement of the colloidal particles. However, typical microfabrication practices, which involve etching the channels on suitable metallic films, rarely yield smooth walls. In many cases, the roughness of the walls is substantial, which adversely influences the manipulation of the particles by altering the electrical field distributions in the channel.

In this study, we present numerical simulation results depicting how such roughness on the confining walls can influence the electrostatic forces on the particles. We assess the EDL interaction force between two colloidal particles located axially in a rough cylindrical capillary employing finite element analysis. The roughness is modeled as a periodic oscillation in the capillary wall radius with various amplitudes and wavelengths, thus emulating a wide variety of roughness features. Since the governing Poisson–Boltzmann (PB) equation is a nonlinear partial differential equation, and the capillary surface has a complex geometry, analytical solutions cannot be obtained. The finite element technique, owing to its ability to handle complex geometrical domains, is one of the possible ways to solve such a problem. The simulations presented here provide considerable insight regarding the electrostatic double-layer forces experienced by spherical particles in rough confinements and indicate possible limitations imposed by channel wall roughness on precise electrokinetic manipulation of nanoparticles in microchannels.

2. Mathematical modeling of spherical particles inside a rough capillary

The behavior of charged particles suspended in an electrolyte inside a charged cylindrical capillary can be analyzed by solving the nonlinear Poisson–Boltzmann equation with appropriate boundary conditions imposed on the charged particle and capillary wall surfaces. In this section, we present a brief description of the mathematical formulation, particularly focusing on the procedures for generating the rough capillary wall, and some key steps used in the numerical solution. A detailed description of the numerical procedure is available elsewhere [22].

2.1. Computational domain, governing equation, and boundary conditions

Fig. 1 shows the cylindrical geometry under consideration in the present investigation along with the coordinate framework. The schematic representation of the particles

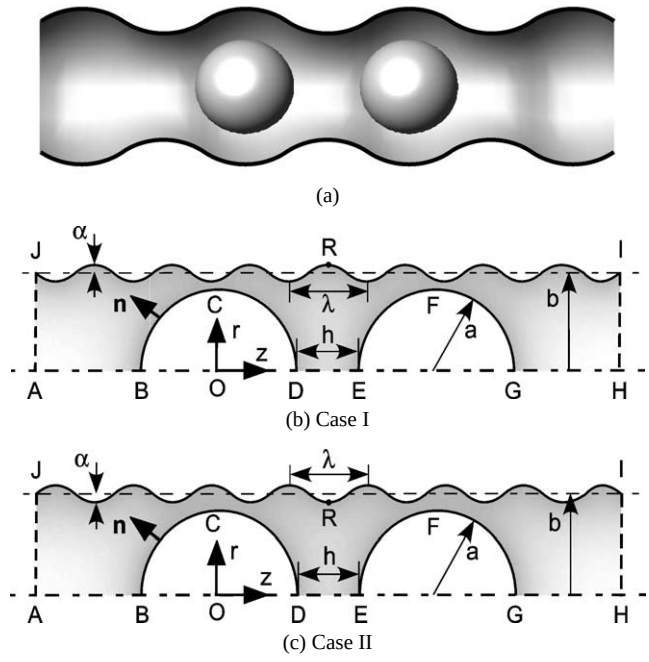

Fig. 1. (a) Schematic representation of the computational domain for two spherical colloidal particles inside a "rough" capillary. (b) Particles are moving uniformly from the crest of an undulation denoted by the point R (case I). (c) Particles are moving uniformly from the trough of an undulation (case II). Utilizing the symmetry around the horizontal axis (AH), the two-dimensional formulation of the governing equation was developed. The arc BCD and arc EFG represent the particle surfaces, while IJ represents the undulation of the capillary. The origin of the cylindrical coordinate system is located at O. The amplitude of the cylinder wall roughness is denoted by α and λ represents the wavelength of the undulation.

enclosed in the rough capillary is given in Fig. 1a, while Figs. 1b and 1c depict the geometric details of the axisymmetric problem discussed in this paper. Here, two spherical colloidal particles of radius a are separated by a distance h (distance of closest approach) in an infinitely long "rough" capillary of mean radius b, pitch (or wavelength) λ, and amplitude α. Two different cases are considered depending on the relative particle position inside the capillary. Case I (Fig. 1b) considers the crest of the undulation (R) as a reference point, while case II (Fig. 1c) considers the trough of the undulating capillary as the reference point. The interaction forces between the particles are determined for each of these cases at various separation distances relative to the reference point R. The ratio of the particle radius to the mean radius of the cylindrical capillary is denoted as the aspect ratio A $(= a/b)$.

Utilizing the axisymmetry when the particles are axially located in the capillary, the governing Poisson–Boltzmann (PB) equation can be written in the cylindrical coordinate system as

$$\frac{\partial^2 \Psi}{\partial \bar{r}^2} + \frac{\partial^2 \Psi}{\partial \bar{z}^2} = \sinh(\Psi) - \frac{1}{\bar{r}} \frac{\partial \Psi}{\partial \bar{r}}, \tag{1}$$

where Ψ $(= ve\psi/kT)$ is the scaled potential, and the scaled coordinates are $\bar{r} = \kappa r$ and $\bar{z} = \kappa z$. The coordinates are scaled with respect to the Debye screening length, κ^{-1}. For a symmetric $(v : v)$ electrolyte, the screening length is

$$\kappa^{-1} = \left(\sqrt{\frac{2 n_\infty e^2 v^2}{\varepsilon \varepsilon_0 kT}} \right)^{-1}, \tag{2}$$

where n_∞ is the bulk concentration of the ions (in numbers/m^3), ε is the dielectric constant of the suspending fluid, ε_0 is the dielectric permittivity of vacuum, e is the fundamental charge, v is the valence of the ions, k is the Boltzmann constant, and T is the absolute temperature.

The particle surfaces may be treated as either constant surface potential (CP) or constant surface charge density (CC) boundaries. In our earlier study [22], both CP and CC cases were considered to evaluate the interaction forces between two spherical colloidal particles inside a charged cylindrical capillary. It was observed that the interaction force between the spheres was affected significantly by the proximity of the charged cylinder wall only for constant surface potential particles. Accordingly, in the present investigation, we consider only CP boundary conditions for the particle and capillary wall surfaces.

The boundary conditions for the problem are (Fig. 1)

$$\Psi = \Psi_p \quad \text{for } \partial\Omega \in \text{ BCD and EFG}, \tag{3a}$$

$$\Psi = \Psi_c \quad \text{for } \partial\Omega \in \text{ IJ}, \tag{3b}$$

$$\mathbf{n} \cdot \nabla \Psi = 0 \quad \text{for } \partial\Omega \in \text{ AB, DE, GH, HI, and JA}. \tag{3c}$$

The last statement, Eq. (3c), provides the symmetry conditions on the fluid boundaries, implying that the potential gradients normal to these line segments are zero. In this equation, **n** represents the unit normal to the surface. Clearly, this is an artificial boundary condition on the segments JA and HI, and appropriate measures must be taken in the numerical solution to ensure that this artificial boundary condition does not influence the accuracy of the solution. To solve Eq. (1) numerically, we used the finite element technique with adaptive mesh refinement as described in our earlier work [22]. The finite element simulations were performed using FEMLAB (COMSOL, Inc.) software running on a MATLab (Mathworks, Inc.) platform in a personal computer (with a 1 GHz Pentium III processor and 1 GB of RAM).

2.2. Generation of a rough surface

In the present investigation, Bézier curves are utilized to generate an undulating roughness pattern on the capillary wall. For a set of $(n + 1)$ control points $P_0, P_1, \ldots, P_n$, the corresponding Bézier curve is given by [23]

$$b(t) = \sum_{i=0}^{n} P_i B_{i,n}(t), \quad t \in [0, 1], \tag{4}$$

where $B_{i,n}(t)$ are Bernstein polynomials, defined as

$$B_{i,n}(t) = \binom{n}{i} t^i (1-t)^{n-i}. \tag{5}$$

For numerical calculations, a rational Bézier curve is defined by

$$b(t) = \frac{\sum_{i=0}^{n} w_i P_i B_{i,n}(t)}{\sum_{i=0}^{n} w_i B_{i,n}(t)}, \quad t \in [0, 1], \tag{6}$$

where n is the order, $B_{i,n}$ are the Bernstein polynomials, P_i are control vertices of the n-dimensional space, and w_i are the weights, which should always be positive real numbers to get a properly defined rational Bézier curve. The Bézier curve always passes through the first and last control points and lies within the convex hull of the control points. One of the most useful properties of the rational Bézier curves is that the direction of the tangent vector at $t = 0$ and $t = 1$ is determined by the vectors $P_1 - P_0$ and $P_n - P_{n-1}$, respectively. In other words, the curve will always be tangent to the line connecting control vertices P_0 and P_1, and also to the line connecting P_{n-1} and P_n. We used quadratic Bézier curves to avoid numerical instability associated with higher order Bézier curves. Three control points are needed to define a quadratic Bézier curve. Considering three control points P_0, P_1, and P_2, a quadratic Bézier curve is defined as

$$b(t) = (1-t)^2 P_0 + 2t(1-t) P_1 + t^2 P_2. \tag{7}$$

Here t is a parameter between 0 and 1, where $b(0) = P_0$ and $b(1) = P_2$, such that the curve passes through the control points P_0 and P_2. The functions $(1-t)^2$, $2t(1-t)$, and t^2 that are used to blend the control points P_0, P_1, and P_2 together are the second degree Bernstein polynomials. Equation (6) is a linear combination of quadratic polynomials, and therefore it represents a parabolic segment. Thus,

the quadratic Bézier curve is simply a continuous parabolic curve and has continuous derivatives of all orders. Substituting Eqs. (5) and (7) in Eq. (6), the final form of the quadratic rational Bézier curve is written as

$$b(t) = \frac{w_0(1-t)^2 P_0 + 2w_1 t(1-t)P_1 + w_2 t^2 P_2}{w_0(1-t)^2 + 2w_1 t(1-t) + w_2 t^2}. \tag{8}$$

Throughout this study, w_0 and w_2 are kept constant to maintain symmetry over the point P_1, while w_1 is varied to control the amplitude of the roughness and the two end or anchor points are used to vary the pitch. If P_1 and w_1 are known, the amplitude of the asperities can be calculated from the following relationship:

$$\alpha = \frac{P_1}{1+w_1}. \tag{9}$$

2.3. Calculation of electrostatic force

Once the potential distribution is obtained by solving the PB equation, the net electrostatic force between the two particles is given by integrating the stress tensor on any arbitrary closed surface. In this study, the stress tensor was evaluated on the surface of one of the spherical colloidal particles. The stress tensor comprises an isotropic osmotic contribution and the Maxwell stresses arising from the electrostatic field. Combining these, the electrostatic force on the spherical colloidal particle is expressed as

$$\begin{aligned}\mathbf{F} &= \iint_S \mathbf{T}_{ij} \cdot \mathbf{n}\, dS \\ &= \iint_S \left[\left(\Pi - \frac{1}{2}\varepsilon\varepsilon_0 \mathbf{E}\cdot\mathbf{E} \right)\mathrm{I} + \varepsilon\varepsilon_0 \mathbf{E}\mathbf{E} \right] \cdot \mathbf{n}\, dS. \end{aligned} \tag{10}$$

Here $\mathbf{F}$ is the force acting on the sphere, $\mathbf{T}_{ij}$ is the electrostatic stress tensor, $\mathbf{E}$ $(= -\nabla\psi)$ is the electrostatic field vector, Π is the osmotic pressure difference between the electrolyte at the particle surface and the bulk electrolyte, $\mathbf{n}$ is the unit outward surface normal, and $\mathbf{I}$ represents the identity tensor.

The net force acting on a sphere along the axial (z) direction can be determined from the component of Eq. (10) acting along the z direction. Utilizing the fact that the integral of the isotropic osmotic pressure term over a closed surface of constant potential is always zero, the force acting along the z direction can be written explicitly as

$$\begin{aligned} F_z &= \mathbf{F}\cdot\mathbf{k} \\ &= 2\pi\kappa^2\varepsilon\varepsilon_0 \left(\frac{kT}{ve}\right)^2 \\ &\quad \times \int_{S_p} \left[n_r E_r E_z + \frac{1}{2} n_z \left(E_z^2 - E_r^2 \right) \right] r\, dr, \end{aligned} \tag{11}$$

where $\mathbf{k}$ is a unit vector in the positive z direction, n_r and n_z are the components of the unit surface normal vector $\mathbf{n}$ along the r and z directions, respectively, and S_p (the arc BCD in this present case) represents the semicircular boundary of the spherical particle over which the integration is performed. E_r and E_z are the components of the electric field vector $\mathbf{E}$ along the r and z directions, respectively. Finally, the axial force is represented in its nondimensional form, given by

$$f_z = \frac{F_z}{\varepsilon\varepsilon_0}\left(\frac{ve}{kT}\right)^2. \tag{12}$$

We note here that since the force is calculated on the sphere BCD with its center at the origin, a repulsive force will be directed toward the negative z direction, while an attractive force will act along the positive z direction. Hence, in the results presented, a negative value of the force will imply repulsion, while a positive value attraction.

3. Electrostatic interaction force on a spherical particle

In this section, we depict the simulation results obtained from the mathematical model described in Section 2. First, to assess the accuracy of the numerical methodology, we compare one of our finite element calculations for the limiting case of two identical charged particles in an infinite electrolyte medium with the corresponding results available elsewhere [17,19]. Following this, we present simulation results for the interaction force experience by a spherical particle inside a rough capillary for various combinations of the roughness parameters to explore the key effects of surface roughness on the interparticle interaction.

3.1. Electrostatic double-layer interaction between two charged particles

To assess the accuracy of the finite element solution procedure, we first provide a comparison of the interaction forces between two similarly charged spheres obtained in this work with the corresponding numerical estimates obtained through a Hermite collocation-based solution of the PB equation in a bispherical coordinate system described elsewhere [17,19]. The results are shown for both constant potential (CP) and constant charge (CC) conditions on the particle surfaces. The charge density used in the CC calculations was based on a scaled surface potential $(ve\psi/kT)$ of -3.0 on the isolated particles, which is related to the scaled surface charge density, σ_p, through [24]

$$\begin{aligned}\sigma_p &= \frac{veq_p}{\varepsilon\varepsilon_0\kappa kT} \\ &= 2\sinh\left(\frac{1}{2}\Psi_{p,\infty}\right) + \frac{4}{\kappa a}\tanh\left(\frac{1}{4}\Psi_{p,\infty}\right), \end{aligned} \tag{13}$$

where q_p is surface charge density $(\mathrm{C/m^2})$ and $\Psi_{p,\infty}$ is the scaled surface potential of an isolated spherical particle.

In the finite element solutions, simulations were carried out for an aspect ratio (a/b) of 0.2 (the mean capillary radius being five times larger than the particle radius) so that the

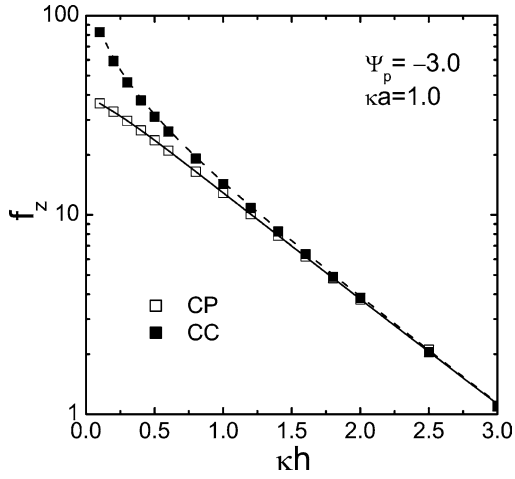

Fig. 2. Comparison between finite element results and the finite difference results based on a Hermite collocation technique in a bispherical coordinate system [17,19]. Symbols represent the finite element results of the electrostatic interaction force between two identical charged particles in an unbounded electrolyte with scaled separation distance (κh) under CP and CC conditions on the particles as indicated in the legend. The lines represent the finite difference collocation results. In the finite element solutions, the charge density on the particles was evaluated employing Eq. (13) for surface potential $\Psi_{p,\infty} = -3.0$, while in the finite difference collocation method it was obtained by numerically solving the PB equation around an isolated particle. The parameter $\kappa a = 1.0$ in this and all subsequent figures.

influence of the capillary wall on the interparticle interaction was minimal. Furthermore, a Neumann boundary condition was applied on the cylinder wall (boundary IJ in Fig. 1):

$$\mathbf{n} \cdot \nabla \Psi = 0 \quad \text{on IJ.} \tag{14}$$

Fig. 2 shows the variation of the scaled interaction force with scaled separation distance between the spherical particles, κh, under CP and CC conditions on the spheres. The open symbols and solid line depict the interaction forces obtained from present investigation and the finite difference results, respectively, for CP conditions on both the particles. The filled symbols and dashed line represent the corresponding results for constant charge condition on the particle surfaces. The finite element results of the present investigation show good agreement with the Hermite collocation results over the entire range of separation distances ($\kappa h = 0.0$–3.0) for both cases. It should be noted that this level of accuracy in the finite element results was attained with adaptive mesh refinement and an appropriate choice of the convergence criterion. In all cases, the scaled forces obtained using the two independent numerical procedures was within 5% of each other.

3.2. Influence of surface roughness on the interaction force

In our earlier study, it was shown that the interaction force between the particles was influenced significantly by the presence of the charged cylinder wall only for constant surface potential particles [22]. Accordingly, in the present study, we have limited our analysis to constant surface potential particles only. The force acting along the axial direction on a spherical particle was determined over wide ranges of the surface roughness on the cylinder governed by the scaled amplitude of the roughness α (defined by amplitude/particle radius), wavelength λ (the pitch of the undulations scaled with respect to particle radius), and different combinations of the surface potentials on the particles and the capillary wall. In the following subsections, the influence of the surface roughness on the electrostatic interaction is discussed for different values of surface potential on the cylindrical capillary.

3.2.1. Particles and capillary with similar surface potentials

The interaction forces between two charged spherical particles inside a charged capillary were calculated for constant potential (CP) boundary conditions when both the particles and the capillary had the same surface potential. The force was determined for the scaled particle–particle separation distance, κh, ranging from 0.0 to 3.0. As mentioned earlier in Section 2, the simulations were performed for two cases: case I corresponding to a reference point (R in Fig. 1b) being at the crest of the rough capillary wall, with the two particles located at equal distances from point R on either side, while case II corresponds to the reference point at the trough (R in Fig. 1c).

Figs. 3 and 4 depict the variation of scaled interaction force with scaled separation distance between the spherical particles (κh) for case I and case II, respectively. The results in both figures correspond to four values of the scaled pitch (wavelength) of the undulation (λ), namely, 0.4, 1.0, 2.0, and 4.0. In all these figures, the force is calculated for a fixed value of the aspect ratio $A = a/b = 0.83$, a fixed dimensionless surface potential $\Psi_p = -3.0$ on the particles and a same dimensionless surface potential on the capillary wall ($\Psi_c = -3.0$). As noted earlier, a negative value of the scaled force in these figures corresponds to repulsion, while a positive value indicates attraction. For comparison, the interaction force between two spheres in an infinitely long smooth cylindrical capillary is depicted as open symbols in each figure.

Fig. 3a indicates that varying the scaled amplitude (α) from 0.05 to 0.15 induces extremely small changes in the magnitude of the scaled electrostatic force compared to a smooth cylinder wall when the scaled wavelength of the undulation ($\lambda = 0.4$) is less than the particle radius ($\kappa a = 1.0$). Irrespective of the value of scaled amplitude, roughness always reduces the repulsive forces between the two colloidal particles at small separation distances. In Figs. 3b, 3c, and 3d, the interaction forces are obtained when the wavelengths of the periodic roughness on the cylinder wall are equal to (Fig. 3b) or greater than (Figs. 3c and 3d) the particle radius. In these cases, we start to observe an oscillatory behavior of the interaction force between the spheres. These oscillations correspond to the periodic nature of the capillary wall roughness, and the extent of the

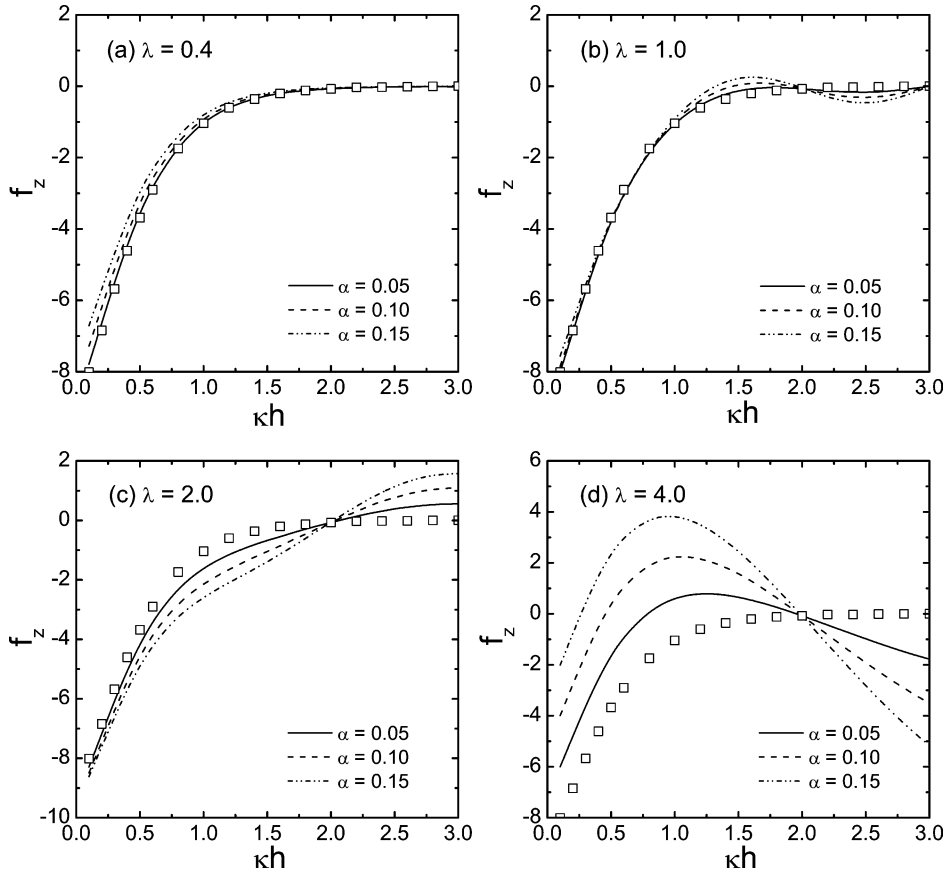

Fig. 3. Variations of the scaled electrostatic interaction force between two spherical particles inside a "rough" capillary with scaled separation distance when the particles are moving uniformly from the crest of an undulation (case I). Both particles and capillary are similarly charged ($\Psi_p = \Psi_c = -3.0$) and different line types correspond to different values of scaled amplitude of the roughness as indicated in the legend. The simulations were performed for four values of scaled wavelength of the undulation, indicated by the four values of λ in parts (a) to (d). The open symbols depict the electrostatic interaction force between two CP particles inside a similarly charged (bearing same surface potential as particles) smooth ($\alpha = 0.0$) cylindrical capillary [22].

oscillations increases with the amplitude of the roughness. For $\lambda = 2.0$ and 4.0, the interaction force even becomes attractive at certain locations, and the particles feel a periodic attractive and repulsive interaction as the separation distance between them is increased. In all cases, the interaction force is primarily contributed by the roughness of the capillary wall, and when the interparticle separation becomes larger than approximately one wavelength of the periodic roughness of the capillary, each spherical particle appears to solely interact with the capillary wall. The behavior described above is strongly dictated by the amplitude of the roughness, larger amplitudes leading to greater oscillations in the interaction force. Furthermore, all the oscillations seem to occur symmetrically about the zero amplitude force.

The forces corresponding to case II when the particles are moving uniformly from the reference point R on the trough of an undulation are shown in Fig. 4, which indicates a different behavior compared to the case I for larger wavelengths of the undulation. These results were obtained under identical parameter settings for the case I simulations. In Figs. 4a and 4b, trends in the interaction forces are observed for small values of λ (< 1.0) similar to those in Figs. 3a and 3b at small separations. Here, surface roughness reduces the magnitudes of the electrostatic repulsion for small separations ($\kappa h \leqslant 0.5$). From these two figures, it is clear that for small λ, the relative position of a particle with respect to the crest or trough of an undulating wall does not play any significant role on the electrostatic interaction. However, the variation of electrostatic force between the particles for $\lambda = 2.0$ and 4.0 are completely opposite both in nature and magnitude when we compare Figs. 3c and 3d to Figs. 4c and 4d. In case I, the interaction force is more repulsive when the separation distance is less than the wavelength for $\lambda = 2.0$, while in case II, the force is less repulsive, and even becomes slightly attractive near $\kappa h = 1.0$ (Figs. 3c and 4c). The trends in Figs. 3d and 4d are exactly opposite to the above observation.

3.2.2. Particles inside a rough capillary with zero surface potential

Figs. 5 and 6 show the variation of the scaled interaction force with scaled separation distance between the spherical particles (κh) for case I and case II, respectively. The simulations of Figs. 5 and 6 were performed under identical conditions as in Figs. 3 and 4, respectively, except for zero

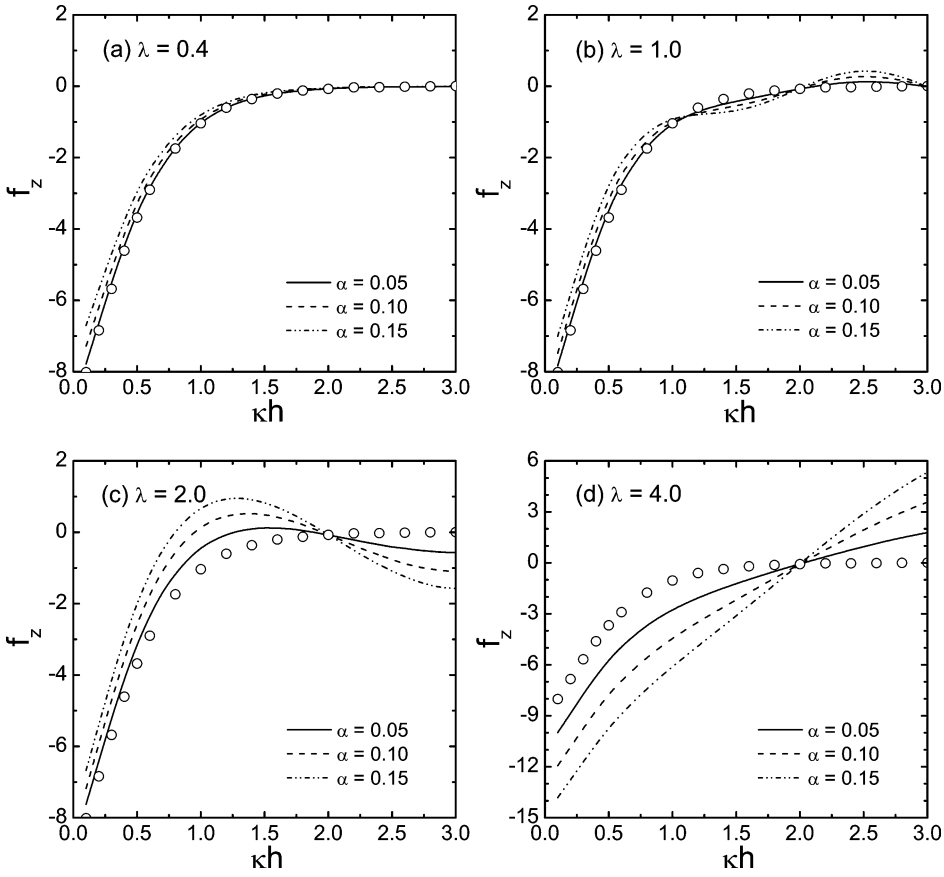

Fig. 4. Scaled electrostatic interaction force between two spherical particles as a function of scaled separation distance when the particles are moving uniformly from the trough of an undulation (case II) under same conditions as in Fig. 3.

surface potential conditions on the capillary wall ($\Psi_c = 0$). The four parts (a–d) in each of these figures correspond to four values of the scaled wavelength of the undulation (λ), namely, 0.4, 1.0, 2.0, and 4.0, respectively. For similarly charged particles and cylinder, we did not observe significant effect of the amplitude on the interaction force in terms of the magnitude (refer to Figs. 3a, 3b and Figs. 4a, 4b), particularly for smaller wavelengths. For different particle and capillary wall surface potentials, however, the effect of amplitude on the interaction force is considerable in terms of the magnitude as well as the nature of the forces even for small wavelengths. For smaller amplitudes ($\alpha < 0.1$), variations of the electrostatic force are negligible compared to the cases when amplitude is higher than 0.1. For large amplitudes, the force is oscillatory, closely emulating the periodic undulations of the capillary wall. Depending upon the relative position of the particles, the forces are either repulsive or attractive. For $\lambda \geqslant 1.0$, a dramatic change in magnitude of the forces is observed even at small amplitudes. A slight increase in amplitude causes a significant enhancement in the interaction force on the particles. The presence of roughness appears to induce a significant oscillation in the forces, which alternately become attractive and repulsive, emulating the periodic nature of the roughness. In sharp contrast, the particles always exhibit a repulsive force inside a smooth capillary. As depicted in Figs. 6a–6d, the nature of the force is opposite when the particles are moving away from the trough of an undulation compared to when the particles are moving away from the crest. For separation distances larger than the wavelength of the roughness, the maxima and minima of the interaction force have nearly identical values (Figs. 5b and 6b).

3.2.3. Particles and capillary wall with oppositely charged surfaces

The interaction forces between the spherical particles were determined so far for situations where the particles and the cylinder surfaces had potentials with same sign (like-charge cases) and the case when the particles had potentials with same sign but the capillary wall surface potential was zero. Figs. 7 and 8 represent the variation of interaction force for cases where the capillary surface is oppositely charged with respect to the particles. The simulations of Figs. 7 and 8 were performed under conditions identical to those in all the previous cases, except for the opposite sign of the surface potential on the capillary wall ($\Psi_c = +3.0$). Fig. 7 shows the simulations for case I (particles moving away from the crest). The four parts (a–d) in Fig. 7 correspond to four values of the scaled wavelength of the undulation (λ) as indicated in the figure. Fig. 8 depicts the corresponding results

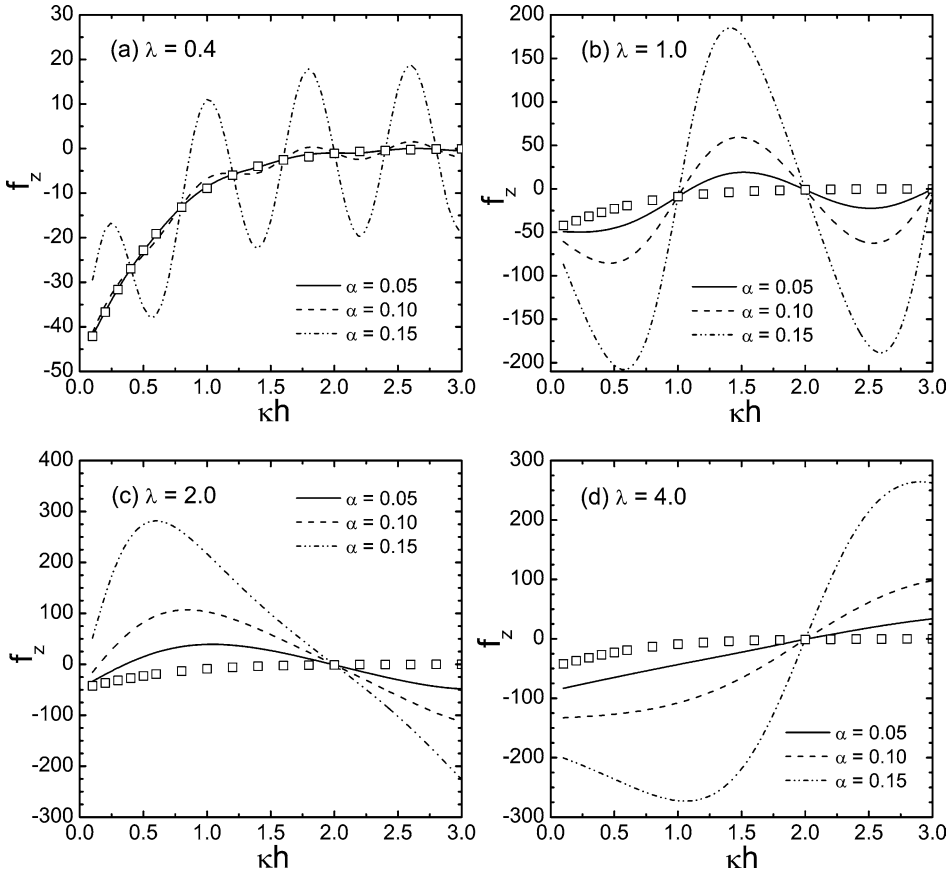

Fig. 5. Variation of the scaled electrostatic interaction force between two similarly charged spherical particles inside an uncharged "rough" capillary with scaled separation distance for case I. Simulations were performed under same boundary conditions as in Fig. 3, except for zero surface potential on the capillary wall ($\Psi_c = 0.0$). The open symbols depict the electrostatic interaction force between two CP particles inside an uncharged (zero surface potential) smooth ($\alpha = 0.0$) cylindrical capillary [22].

for case II with all other parameters identical to the simulations of Fig. 7. Both these results follow qualitative behavior similar to that in the corresponding simulations for the cylinder wall with zero surface potential, although the magnitude of the interaction force was found to be considerably larger than in the preceding case. From these results, it is evident that the roughness effects of the oppositely charged capillary wall are so pronounced that the particle–particle interaction force is strongly oscillatory even at very small interparticle separations.

4. Discussion

The results from the previous section throw considerable light on the behavior of the electrostatic double-layer force experienced by a spherical colloidal particle inside a rough capillary, which is charged to different extents. The most striking feature of these results is the enormous influence of the capillary wall roughness on the magnitude and sign of the interaction force. In this section we discuss some of the implications of these roughness engendered oscillatory forces on the behavior of nanoparticles confined in capillary cavities.

The simulations presented here all represent situations where the particle and cylinder mean radii are comparable to the screening length of the electrostatic double-layer interactions. Furthermore, all the calculations were for comparable particle and cylinder radii corresponding to the scenario of particles confined in tightly fitting capillaries. The dramatic oscillatory behavior observed in such tightly fitting pores decay sharply as the aspect ratio (a/b) is decreased, and for aspect ratios of about 0.5, the oscillations are imperceptible. Similarly, the oscillations in the force are damped dramatically as the particle size to screening length ratio, κa, is increased. We should also note that the large variations noted here are only observed for constant potential particles. For constant charge density on the particle surfaces, the influence of roughness is not so dramatic.

The interaction force experienced by a spherical particle in rough capillaries evolves from two competing factors. First, presence of the similarly charged (implying same sign of the surface potential as the particle surface potential) smooth cylinder wall causes a reduction in the interaction force compared to the force between two particles in an infinite domain. This can be observed by comparing the constant potential results of Fig. 2 with the zero amplitude forces (symbols) in Fig. 3. Secondly, oscillations in the capillary

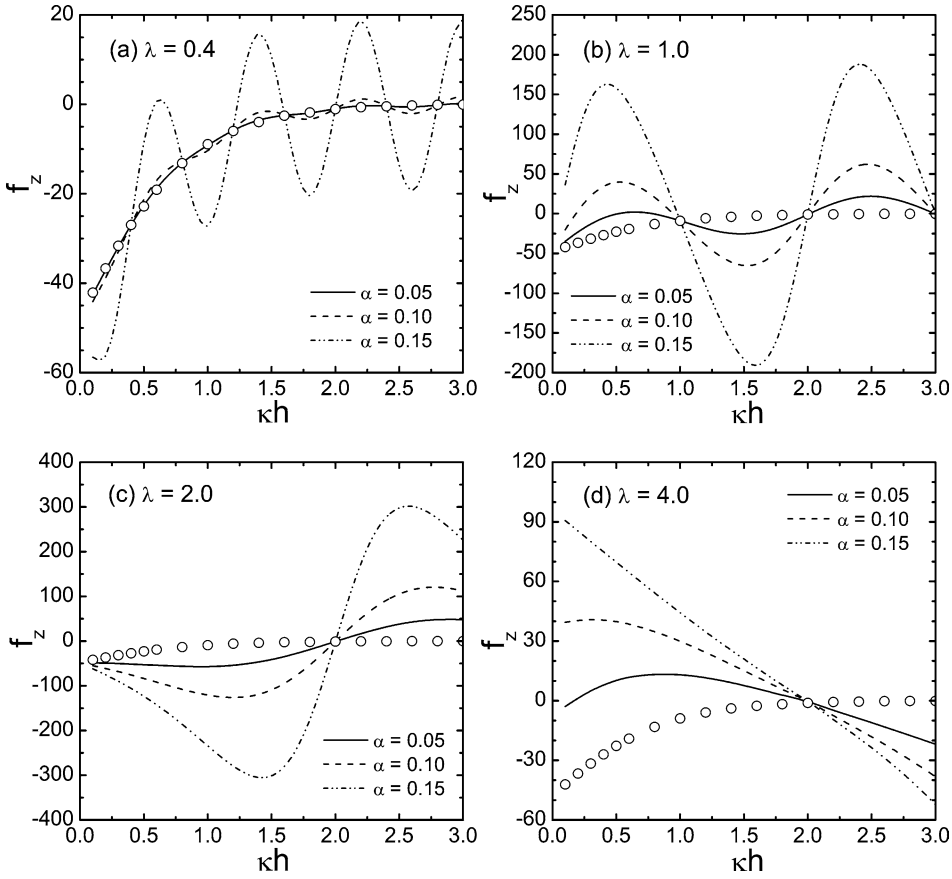

Fig. 6. Variation of the scaled electrostatic interaction force between two similarly charged spherical particles inside an uncharged "rough" capillary with scaled separation distance for case II under same conditions as in Fig. 5.

wall result in severe modifications of the electrostatic stress tensor by imposing unbalanced Maxwell stresses on the particle due to asymmetry in the rough cylinder geometry. The periodic nature of the interaction force exactly matches the wavelength of the undulations in the capillary wall. When both the particles and cylinder surfaces have the same surface potentials (both magnitude and sign), the magnitude of the force is small. However, the forces are drastically enhanced as the cylinder surface potential changes from the sphere surface potential. In absence of roughness, reducing the surface potential of the cylinder wall substantially enhances the repulsion between the spherical particles. If, in addition, the amplitude of the roughness is increased, the repulsion is increased even further. However, the repulsion is caused solely by the asymmetric positioning of regions of the cylinder wall in the vicinity of the spherical particle. The effect of such asymmetric stresses induced by the wall with different surface potentials on the sphere is so intense that even at very small separations between the particles, we start observing a considerable oscillation of the interaction force (note the distinct differences between the interaction forces in Figs. 3a, 5a, and 7a for small κh). In other words, for dissimilar surface potentials on the spheres and the cylinder, the interaction force between the spheres is predominantly dictated by the charge and periodicity of the cylinder wall surface. The force oscillates around a mean value that represents the particle–particle interaction in a smooth cylindrical capillary, with a superimposed oscillation that follows the pattern of the cylinder wall.

Noting that for constant potential particles, the osmotic stress has no influence on the total interaction force, it is discernable that the force variations are only caused by the modification of the Maxwell stresses brought about by modification of the electrostatic fields. Forcing the cylinder surface potentials to different values compared to the sphere surfaces alters the electric fields at the sphere surfaces quite dramatically. The modification of these fields and the Maxwell stresses are most prominent near the points of closest approach between the sphere and the cylinder surfaces. Thus, the oscillations in the force are primarily an outcome of the local electrostatic field modifications. We should note, however, that the magnitudes of the force oscillations obtained for oppositely charged capillaries may be unrealistically high. This high value is an artifact of our use of the Boltzmann distribution and assumption of point charge ions in our analysis. Such an approximation allows concentration of extremely large number of ions near the troughs of the undulating cylinder wall, which is physically unrealistic. Although we do not report studies including the effects

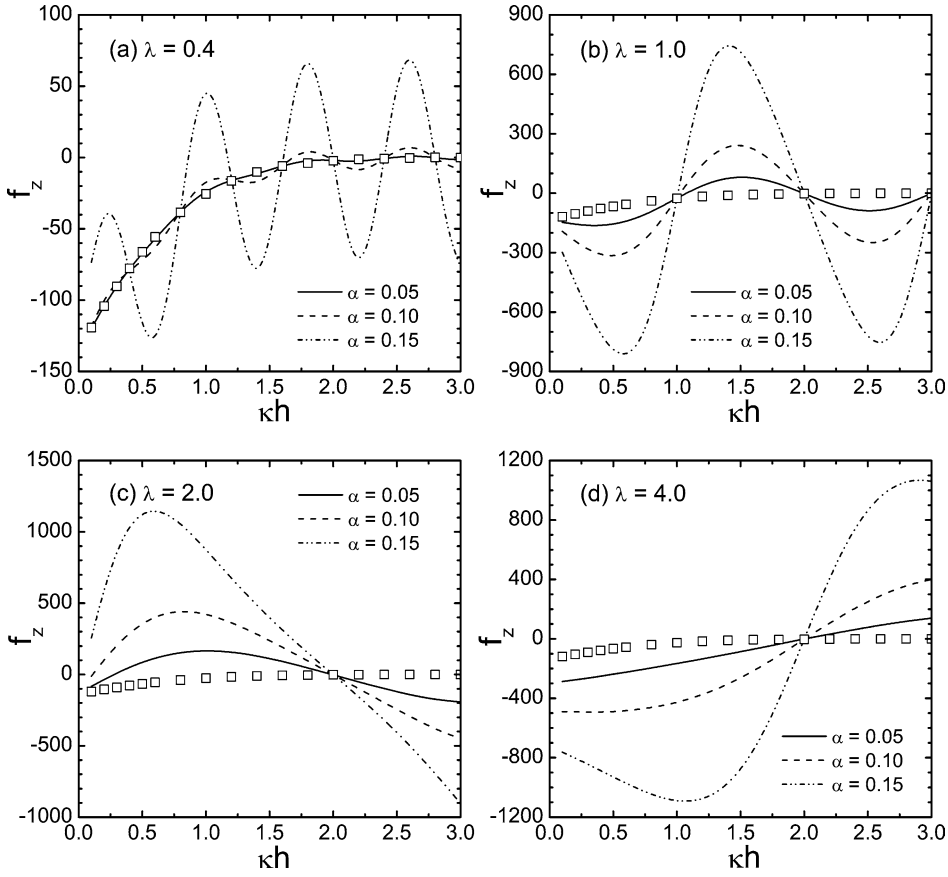

Fig. 7. Variation of the scaled particle–particle interaction force between two similarly charged spherical particles inside an oppositely charged ($\Psi_c = -\Psi_p$) capillary with scaled separation distance for case I. The scaled surface potential on the capillary wall is $\Psi_c = +3.0$, while the particle surface potential is given by $\Psi_p = -3.0$. All other parameters are same as in Fig. 3. The open symbols depict the electrostatic interaction force between two CP particles inside an oppositely charged smooth ($\alpha = 0.0$) cylindrical capillary [22].

of finite ion sizes, it is believed inclusion of such effects will result in a more modest variation of forces.

The oscillatory force experienced by the spherical particle is possible only in case of nanoscale particles and may be instrumental in dictating the transport behavior of nanoparticles in confined geometries of comparable dimensions. In these situations, the roughness of the confining wall (and, of course, the surface texture of the particles themselves) becomes comparable to the scaled amplitude values employed in these simulations. For instance, if we consider a 50-nm-radius colloidal particle in a 60-nm-radius cylinder, a scaled amplitude of 0.1 will indicate that the roughness is of the order of 5 nm.

This scale of roughness can be obtained quite readily in photolithographic microfabrication of microchannels by etching a sputtered metal layer on a silicon wafer. The purpose of etching a metal film is to produce channels, the walls of which can be charged up to a constant surface potential. Although silicon or glass substrates can be etched to a considerably higher precision than metal films, we cannot form constant potential surfaces on these materials. Typical results obtained from etching an aluminum film using a wet-etching process are depicted in Fig. 9. Fig. 9a shows an array of approximately 6-μm-wide rectangular channels scanned using an atomic force microscope (Digital Instruments' Dimension 3100 SPM). The depth of these channels is approximately 450 nm. The unevenness of the metal film, particularly at the vertical walls, is readily visible in this image. A quantitative depiction of the extent of roughness on these vertical sidewalls is possible through a width analysis performed on the individual channels. Fig. 9b shows a typical section over which the analysis is performed.

In AFM width analysis, we measure the average width of a feature inside a specified box (shown by the rectangle in Fig. 9b). The average width is obtained by measuring the lengths of all the line segments aligned parallel to the horizontal sides of the box (the horizontal scan lines). The standard deviation of this width distribution provides an estimate of the vertical wall roughness. We performed this analysis on three consecutive channels in a wafer. For each channel, the mean width and standard deviation were measured at four different vertical locations (100, 200, 300, and 400 nm) in the channel. Similar measurements were also conducted using another wafer where the channel width was 5 μm. The measurement results are summarized in Table 1. From this table, we note that the channel width decreases with depth in all cases. In other words, the channels are slightly tapered.

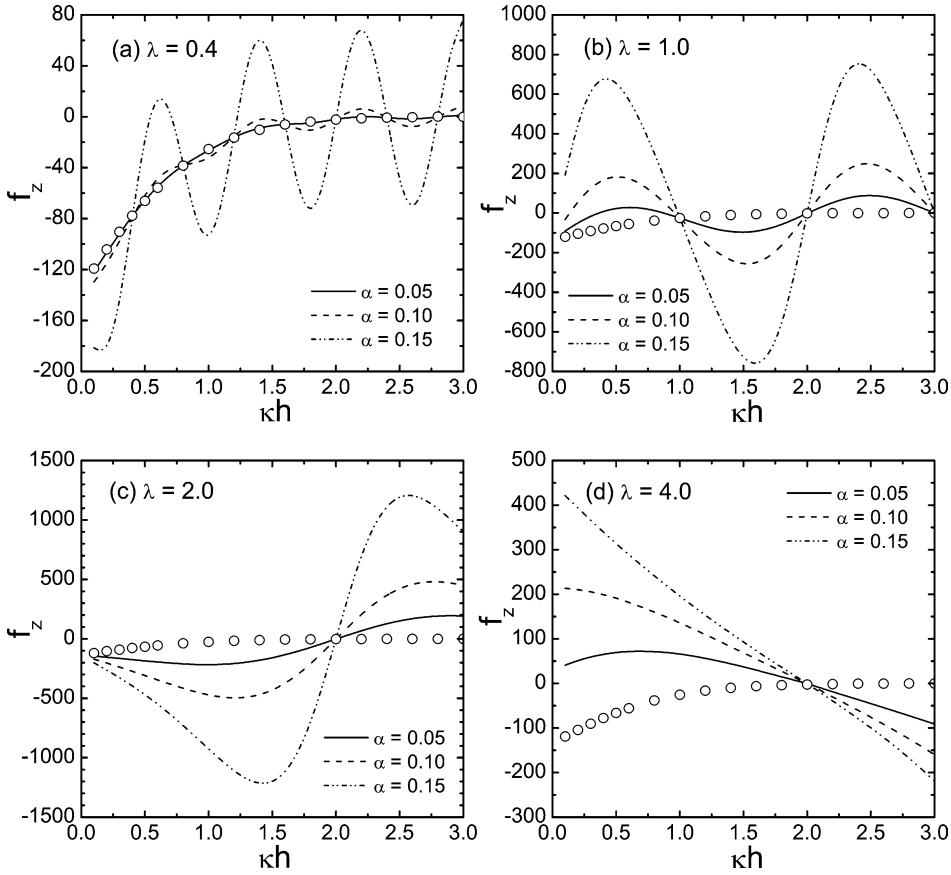

Fig. 8. Variation of the scaled particle–particle interaction force between two similarly charged spherical particles inside an oppositely charged capillary with scaled separation distance for case II under the same conditions as in Fig. 7.

Table 1
Width analysis statistics from atomic force microscope scans of rectangular microchannels

Channel	Threshold (nm)	100	200	300	400
		Wafer 1: channel width = 6 μm, channel height = 453 nm			
1	Mean width	6140	6319	6460	6595
	Std. deviation	80.10	79.35	85.10	85.58
2	Mean width	6305	6480	6630	6769
	Std. deviation	90.02	86.57	78.84	79.24
3	Mean width	6301	6474	6622	6757
	Std. deviation	80.57	80.80	78.33	82.82
		Wafer 2: channel width = 5 μm, channel height = 449 nm			
1	Mean width	5000	5220	5390	5537
	Std. deviation	96.98	89.06	86.87	82.43
2	Mean width	5098	5312	5488	5635
	Std. deviation	93.23	89.03	80.72	75.74
3	Mean width	4897	5110	5280	5422
	Std. deviation	83.03	74.03	74.46	72.37

Two different wafers with different channel widths but same channel height were analyzed. The threshold value represents the vertical height from the base of the channel.

Second, the standard deviation, which provides a measure of the roughness, does not depend on the channel width. The average standard deviation from all these measurements was determined as 82.72 nm. The standard deviation, to a good approximation, represents the sum of the roughness amplitudes from the two vertical walls of a channel. Assuming that the average roughness on both the sidewalls are same, we estimate the roughness amplitude on a channel wall to be 41.36 nm.

The above analysis reveals that the mean roughness of wet-etched metal film channels that are about 450 nm deep is on the order of 40 nm. Scaling this information linearly to 100-nm-deep channels yields a value of about 10 nm for the wall roughness. Therefore, it is clearly discernable that

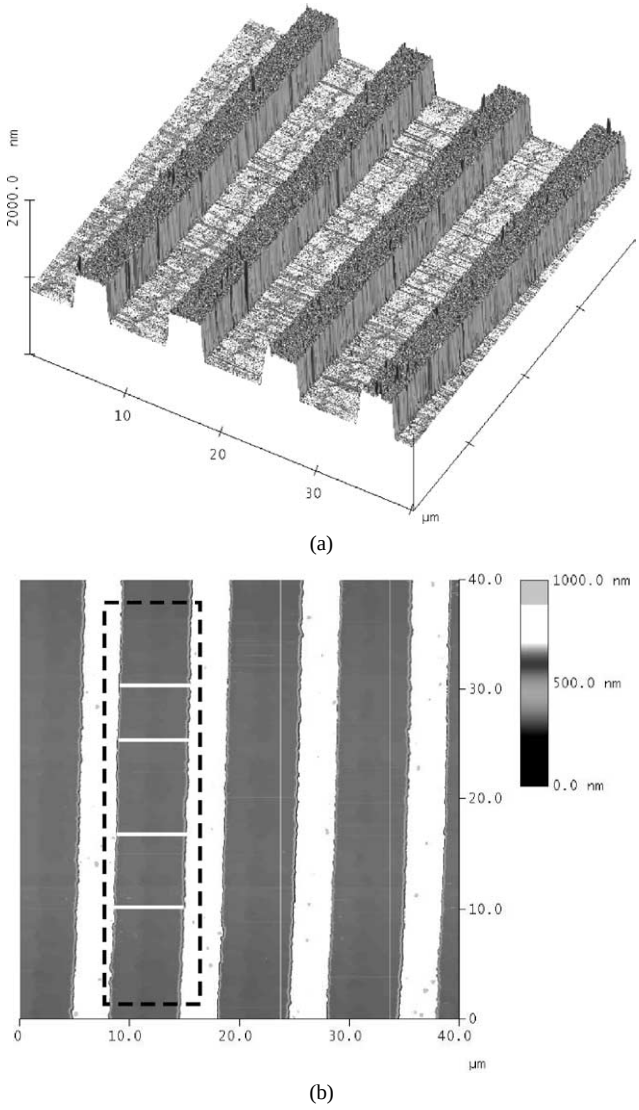

Fig. 9. Atomic force microscope (AFM) image of microfabricated rectangular channels showing the procedure of measuring surface roughness by width analysis. (a) Pattern showing an array of 6-μm-wide and ca. 0.45-μm-deep rectangular microchannels etched on an aluminum film. (b) Top view of patterned surface showing the section over which the width analysis is performed. The dashed rectangular box is placed on each channel and the width of the channel is measured by recording the lengths of all the horizontal scan lines (horizontal white lines) spanning the width of the channel. The measurements are performed at different channel heights.

the roughness amplitudes considered in this study are comparable to those obtainable in microfabrication processes. In top-down microfabrication processes, we will generally obtain significant roughness on the walls of these channels, which in turn, can considerably affect the electrostatic interaction of a charged particle that is comparable in dimension to the channel depth. Although the channels in the above discussion are rectangular, the analysis performed using the cylindrical geometry in our simulation studies provides considerable insight regarding the qualitative behavior of the interactions experienced by particles near the axis of these rectangular channels.

5. Concluding remarks

The simulations performed in this study reveal that the electrostatic double-layer interaction force experienced by a spherical colloidal particle inside a "rough" capillary can be significantly modified by the roughness of the capillary wall. The influence of the wall roughness is significant when the periodicity of the roughness (wavelength) is comparable to or larger than the particle radius. When the periodicity of the roughness is considerably smaller than the particle dimension, the interaction force experienced by the particle is not seriously altered if both the particles and the cylinder surfaces are similarly charged (bearing the same sign of the surface potential). However, as the cylinder surface potential starts to deviate from the particle surface potential, we observe a considerable influence of the cylinder wall on the electrostatic force experienced by a particle irrespective of the scale of the wall roughness. It is observed that confining charged spherical nanoparticles inside an oppositely charged rough cylinder causes a large fluctuation in the interaction force on the particles. The interaction force felt by a particle in such cases can become attractive or repulsive depending on the axial location of the particle in the rough capillary channel. The roughness amplitudes considered in these simulations appear to be consistent with roughness dimensions generated in photolithographic fabrication of microchannels by etching metal films. Accordingly, it seems that a roughness analysis of the channel walls is a fairly important criterion for correctly assessing the electrokinetic transport behavior of nanoparticles inside such capillaries, particularly when the particle dimensions are comparable to the channel hydraulic diameter.

Acknowledgment

Financial support for this research from the Canada Research Chairs (CRC) program, the Canada Foundation for Innovation (CFI), and the Alberta Ingenuity Fund is gratefully acknowledged. P.K.D. acknowledges a studentship award from the Alberta Ingenuity Fund. We thank Dr. Walied Moussa for allowing us to run the computations on his FEMLab software.

Appendix A. Nomenclature

a	Particle radius
A	Aspect ratio ($= a/b$)
b	Mean capillary radius
$b(t)$	Bézier polynomials
$B_{i,n}(t)$	Bernstein polynomials
e	Electronic charge (1.6×10^{-19} C)
$\mathbf{E}$	Electrostatic field vector
E_r, E_z	Components of the electric field vector along the r and z directions, respectively

$\mathbf{F}$	Force
f_z	Scaled force acting along the z direction
F_z	Component of force acting along the z direction
h	Surface-to-surface separation distance between two spherical particles
i	Index number (0 to n)
$\mathbf{I}$	Identity tensor
k	Boltzmann constant ($1.38 \times 10^{-23}\,\mathrm{J\,K^{-1}}$)
$\mathbf{k}$	Unit vector in the positive z direction
n	Order of the polynomial
$\mathbf{n}$	Unit surface normal vector
n_∞	Ionic number concentration in the bulk solution ($\mathrm{m^{-3}}$)
n_r, n_z	Components of the unit surface normal along the r and z directions, respectively
P_i	Control vertices of a Bézier polynomial
q_p	Surface charge density ($\mathrm{C\,m^{-2}}$)
r	Radial coordinate in the cylindrical coordinate system
$\bar{r}$	Scaled radial coordinate, κr
S_p	Semicircular boundary of the spherical particle
T	Absolute temperature (K)
T_{ij}	Component of stress tensor
w_i	Weights of a rational Bézier polynomial
z	Axial coordinate in the cylindrical coordinate system
$\bar{z}$	Scaled axial coordinate, κz

Greek symbols

α	Scaled amplitude
$\partial\Omega$	Boundary of the computational domain
ε_0	Dielectric permittivity in vacuum ($8.8542 \times 10^{-12}\,\mathrm{C^2\,N^{-1}\,m^{-2}}$)
ε	Dielectric constant of electrolyte
κ	Inverse Debye screening length, Eq. (2)
λ	Scaled wavelength
v	Absolute value of the valency for a symmetric (v:v) electrolyte solution
Π	Osmotic pressure
σ_p	Scaled surface charge density of particle
ψ	Electric potential (V)
Ψ	Scaled potential ($ve\psi/kT$)
$\Psi_p\Psi_c$	Scaled surface potentials of particle and capillary, respectively
$\Psi_{p,\infty}$	scaled surface potential of an isolated spherical particle

Abbreviations

CC	Constant charge
CP	Constant potential
DLVO	Derjaguin–Landau–Verwey–Overbeek
EDL	Electrostatic double layer
LW	Lifshitz–van der Waals
PB	Poisson–Boltzmann

References

[1] B.V. Derjaguin, L. Landau, Acta Physicochim. (USSR) 14 (1941) 633.
[2] E.J. Verwey, J.T.G. Overbeek, Theory of Stability of Lyophobic Colloids, Elsevier, Amsterdam, 1948.
[3] J.H. Masliyah, Electrokinetic Transport Phenomena, AOSTRA, Edmonton, 1994.
[4] M. Elimelech, J. Gregory, X. Jia, R. Williams, Particle Deposition and Aggregation: Measurement, Modeling and Simulation, Butterworth–Heinemann, Oxford, 1995.
[5] A.M. Lenhoff, Colloids Surf. A Physicochem. Eng. Aspects 87 (1994) 49.
[6] S. Bhattacharjee, C.H. Ko, M. Elimelech, Langmuir 14 (1998) 3365.
[7] H. Tamai, Y. Nagai, T. Suzawa, J. Colloid Interface Sci. 91 (1983) 464.
[8] J. Czarnecki, Adv. Colloid Interface Sci. 24 (1986) 283.
[9] J. Czarnecki, P. Warszynski, Colloids Surface 22 (1987) 207.
[10] J.E. Tobiason, Colloids Surface 39 (1989) 53.
[11] M. Elimelech, C.R. Omelia, Langmuir 6 (1990) 1153.
[12] S.Y. Shulepov, G. Frens, J. Colloid Interface Sci. 170 (1995) 44.
[13] S.Y. Shulepov, G. Frens, J. Colloid Interface Sci. 182 (1996) 388.
[14] J.Y. Walz, Adv. Colloid Interface Sci. 74 (1998) 119.
[15] S.L. Carnie, D.Y.C. Chan, J. Colloid Interface Sci. 155 (1993) 297.
[16] S.L. Carnie, D.Y.C. Chan, J.S. Gunning, Langmuir 10 (1994) 2993.
[17] S.L. Carnie, D.Y.C. Chan, J. Stankovich, J. Colloid Interface Sci. 165 (1994) 116.
[18] D. McCormack, S.L. Carnie, D.Y.C. Chan, J. Colloid Interface Sci. 169 (1995) 177.
[19] J. Stankovich, S.L. Carnie, Langmuir 12 (1996) 1453.
[20] P. Warszynski, Z. Adamczyk, J. Colloid Interface Sci. 187 (1997) 283.
[21] S. Bhattacharjee, A. Sharma, J. Colloid Interface Sci. 171 (1995) 288.
[22] P.K. Das, S. Bhattacharjee, W. Moussa, Langmuir 19 (2003) 4162.
[23] E.V. Shikin, A.I. Plis, Handbook on Splines for the User, CRC Press, Boca Raton, FL, 1995.
[24] W.B. Russel, D.A. Saville, W.R. Schowalter, Colloidal Dispersions, Cambridge Univ. Press, Cambridge, UK/New York, 1989.